Novel Four-Port Diplexer–Antenna System with Simultaneous Isolation Enhancement and Impedance Control

Saad Wasmi Osman Luhaib, Farhad E. Mahmood, and Shamil H. Hussein

***Abstract*—This paper presents the design and simulation-based performance evaluation of a novel four-port diplexer–antenna system that simultaneously achieves high transmit/receive isolation and robust impedance control. Two compact parallel-coupled microstrip bandpass filters operating at 2.0 GHz (Rx) and 2.4 GHz (Tx) were synthesized using Chebyshev low-pass prototypes and umerically modeled on a Rogers substrate RO3006 (ϵ_r = 6.5, h = 1.27 mm, tanδ = 0.002). The filters were integrated into a four-port diplexer topology employing a 180^o phase-inversion path to exploit amplitude-and-phase cancellation, thereby reducing filter order and insertion loss while enhancing port-to-port isolation. Full-wave simulations and parametric analyses reveal that the proposed design yields an isolation of 50 dB at 2 GHz and 78.5 dB at 2.4 GHz, representing a substantial improvement over conventional single-filter configurations. Furthermore, the system's isolation performance was evaluated under realistic antenna impedance variations; results show the design retains high isolation despite shifts in both the real and imaginary components of the antenna impedance, with the Tx port demonstrating particularly strong resilience near the matched condition. These findings verify that the co-optimized diplexer–antenna approach effectively mitigates impedance mismatch effects, offering a compact and low-loss solution for modern multi-band wireless front ends requiring stringent Tx/Rx isolation.**

***Index Terms*—Four-Port Diplexer, High isolation, Impedance control, communication systems.**

I. Introduction

MODERN wireless systems increasingly demand devices that integrate antenna interfaces and multi-band/duplexing/trunking front ends with minimal footprint, high efficiency, and strict isolation between transmit (Tx) and receive (Rx) paths to prevent interference and desensitization. Traditional diplexer-antenna systems often employ three-port diplexers coupled to a single antenna, where isolation between the Tx and Rx branches is achieved chiefly via high-order filtering, isolation networks, or large physical separation; such approaches increase complexity, loss, size, or cost [1]– [2].

Manuscript received November 10, 2025; revised December 9, 2025. Date of publication March 30, 2026. Date of current version March 30, 2026.

S. W. Osman Luhaib is with the Department of Electrical Engineering, College of Engineering, University of Mosul, Mosul, Iraq (e-mail: s.w.o.luhaib@uomosul.edu.iq).

F. E. Mahmood and S. H. Hussein are with the Department of Communications and Intelligent Digital Systems Engineering, College of Engineering, University of Mosul, Mosul, Iraq (e-mails: farhad.m@uomosul.edu.iq, Shamil_alnajjar84@uomosul.edu.iq).

Digital Object Identifier (DOI): 10.24138/jcomss-2025-0217

Classical antenna–diplexer integrations rely on three-port diplexers feeding a common antenna, where inter-band isolation is obtained primarily via steep stop-bands from high-order bandpass filters and, in some cases, auxiliary isolation networks [3]. This pathway scales poorly: higher order increases footprint, conductor/dielectric loss, and sensitivity to layout tolerances; moreover, once the antenna presents a non-ideal load, the nominal filter-only isolation degrades and desensitizes the receiver. This size–loss–robustness trade-off in three-port architectures is widely acknowledged and motivates alternative topologies that do not depend solely on brute-force selectivity.

The integration of diplexers/duplexers with a shared antenna has been the subject of extensive research driven by the need to reduce front-end size and cost while maintaining stringent transmit/receive isolation requirements. Building on cancellation concepts, Konpang et al. introduced a four-port diplexer topology that combines two back-to-back three-port diplexers with a 180° phase shift in one branch to obtain large Tx/Rx isolation (≈40 dB) with only second-order filters, thereby reducing filter complexity and insertion loss compared with high-order single-ended solutions [1].

A second line integrates diplexing into the radiator. Self-diplexing and cavity/SIW (substrate-integrated waveguide) antennas route bands to different ports via modal or spatial orthogonality, yielding strong intrinsic co-site isolation for tight band spacing, at the expense of constraints on bandwidth, polarization purity, and fabrication complexity [4]. When antennas and filters are co-optimized, slot engineering and cavity loading can deliver high isolation while sharing a single aperture; however, post-fabrication tuning is limited, and radiation efficiency/mutual-coupling trade-offs become central in compact platforms or MIMO arrays. Reported antenna–diplexer integrations confirm the potential of multi-port topologies for coexistence in crowded spectrum, while underscoring the need to manage efficiency and coupling.

A third thread studies robustness to antenna mismatch. Isolation nulls produced by cancellation networks are load-dependent; small deviations in antenna resistance or reactance retune amplitude/phase balance and collapse isolation. Prior work proposes impedance-tracking balance networks, tunable matching, or calibration loops to restore balance under user loading, manufacturing spread, or multi-band operation—yet many results report only nominal 50 Ω performance or limited

sensitivity maps. Your manuscript positions itself here: it co-optimizes the four-port cancellation network with the antenna interface and a controllable load, and explicitly characterizes isolation under realistic impedance sweeps. In simulations, the structure achieves 50 dB isolation at 2.0 GHz and 78.5 dB at 2.4 GHz, and the isolation trend with R_A swept 40–60 Ω is documented, clarifying which branch (Tx vs. Rx) is more sensitive around match. These observations align with and extend prior robustness discussions by turning them into a concrete impedance-aware design and evaluation protocol.

Parallel lines of research have exploited amplitude-and-phase cancellation using dual-mode or multi-resonator architectures to produce compact diplexers with exceptional port isolation; these works demonstrate that careful resonator/Q engineering and deliberate phase delay enable deep nulls in leakage between closely spaced Tx and Rx bands without resorting to bulky duplexing hardware [5], [6]. Complementary approaches embed the diplexing function into the antenna itself (self-diplexing/self-quadplexing SIW and cavity-backed designs), which can yield high intrinsic port isolation by spatially or modal-orthogonalizing radiating modes, though such solutions often impose constraints on bandwidth, polarization and fabrication complexity [7], [8]. Recent antenna-centric designs have also targeted extremely high co-site isolation for small frequency ratios and tightly spaced bands through slot-engineering and cavity loading, showing that antenna topology and diplexer/filter design must be co-optimized to achieve real-world performance under mismatch and platform effects [2], [9]. Importantly, several studies have highlighted that isolation achieved by ideal cancellation topologies degrades rapidly under realistic antenna impedance variation (due to user loading, manufacturing tolerances, or multi-band operation), prompting the development of impedance-tracking balance networks, tunable matching networks and closed-loop calibration to restore balance and maintain high isolation across frequency and load variations [10], [11].

In radio frequency in acoustic (RF-acoustic) and surface acoustic wave (SAW) domain, phase-cancellation circuits have been used to improve duplexer rejection where filter asymmetries exist, reinforcing the role of precise phase and amplitude control for practical isolation enhancement [11]. Work on four-port microstrip diplexers and compact MIMO antenna–diplexer integrations further demonstrates that multi-port network topologies can be exploited to reject adjacent-band interference and to facilitate coexistence in crowded spectrum environments, but such designs require careful management of mutual coupling and radiation efficiency trade-offs [7], [12]. Taken together, this body of literature establishes three operative design guidelines for a practical four-port diplexer–antenna system: (i) employ amplitude/phase cancellation topologies to obtain deep passive isolation without high filter order [1], [5], (ii) incorporate impedance-tracking or tunable balance/matching networks to make cancellation robust to antenna mismatch and environment-induced impedance shifts [10], [11], and (iii) co-design antenna topology and diplexer/filter resonators (including self-diplexing SIW/cavity approaches) when stringent size, isolation, and multi-band radiation requirements coexist [2], [8], [13].

Building upon these foundations, this work introduces a four-port diplexer–antenna system with simultaneous isolation enhancement and impedance control, in which the four-port diplexer is realized on a Rogers substrate RO3006 (ϵ_r=6.5, h=1.2 mm, tanδ=0.002) to ensure low-loss operation and stable dielectric properties; the bandpass filters employed within the diplexer adopt a parallel-line configuration to achieve compactness and sharp selectivity. The proposed structure is modeled and optimized using AWR Microwave Office to accurately predict S-parameters, impedance behavior, and electromagnetic coupling effects. This design explicitly integrates impedance-control mechanisms at the antenna interface, thereby maintaining high transmit–receive isolation even under realistic VSWR and platform-induced impedance perturbations, and is supported by rigorous analytical derivations as well as full-wave simulations and experimental measurements that collectively quantify the attainable isolation improvement and validate the proposed topology under practical conditions.

Robustness to antenna mismatch remains a critical gap. Deep isolation nulls produced by cancellation networks are load-dependent. Therefore, in this paper, we conduct these concerns by providing the following points:

- A proposed compact 4-port diplexer antenna front-end is designed using a single second-order microstrip bandpass filter and a phase-inversion path (180°), achieving high passive Tx/Rx isolation with low footprint and low loss.
- The proposed antenna structure with interface is co-designed to maintain high isolation under impedance mismatch and a tunable load at the sensing port.
- A complete synthesis and simulation-based realization flow is presented, from Chebyshev filter prototypes to coupled-line microstrip realization on a higher substrate, with full circuit optimization.

The remainder of this paper is organized as follows: Section II describes the design of the parallel-line BPF synthesis methodology. Section III presents the simulation results of the designed filter and the integrated four port diplexer. Section IV analyzes the impact of antenna impedance mismatch on the TX/RX isolation. Section V discusses the main design insights and the robustness trend. Finally, the conclusions are summarized in Section VI.

II. Design Parallel-line BPF Methodology

The parallel-line bandpass filter (BPF) used in the four-port diplexer is designed according to the well-established low-pass prototype transformation and coupled-line synthesis method, augmented by full-wave optimization to account for substrate and fabrication effects. The process begins by specifying the center frequency f_0, the desired fractional bandwidth FBW, the number of order N, and the passband ripple or return-loss requirement. From the Chebyshev low-pass prototype, normalized element values g_0, g_1,…,g_{N+1} are extracted from standard tables [1], [10]. The fractional bandwidth is then calculated as

$$\text{FBW} = \frac{f_h - f_l}{f_0} \tag{1}$$

where f_l and f_h are the lower and upper passband edges. The inter-resonator coupling coefficients ($k_{i,i+1}$) are obtained by [1], [10]

$$k_{i,i+1} = \frac{\text{FBW}}{\sqrt{g_i g_{i+1}}} \tag{2}$$

and the external quality factors (which define the input and output coupling) are

$$Q_{(i-1,i)} = \frac{g_{(i-1)} g_i}{\text{FBW}} \tag{3}$$

Each resonator section is realized as a quarter-wavelength (λ_g/4) edge-coupled line at the center frequency f_0. The physical length ℓ of each resonator on the substrate is [1], [14]–[17]

$$\ell = \frac{\lambda_g}{4} = \frac{c}{4 f_0 \sqrt{\varepsilon_{\text{eff}}}} \tag{4}$$

where c is the speed of light in vacuum and ε_{eff} is the effective dielectric constant of the microstrip, approximated using the Hammerstad–Jensen relation [1], [10]

$$\varepsilon_{eff} = \frac{\varepsilon_r + 1}{2} + \frac{\varepsilon_r - 1}{2}(1 + 12\frac{h}{W})^{-0.5} \tag{5}$$

The characteristic impedance of a single microstrip line is then

$$Z_c = \frac{60}{\sqrt{\varepsilon_{\text{eff}}}} \ln\left[\frac{F}{W/h} + \sqrt{1 + \left(\frac{2}{W/h}\right)^2}\right] \tag{6}$$

Where

$$F = 6 + (2\pi - 6) exp^{-\left(\frac{30.666}{W/h}\right)^{0.7528}} \tag{7}$$

including further corrections for very wide lines [1]. Once the coupling coefficients $k_{i,i+1}$ are determined, the impedance of even-mode Z_{0e} and odd-mode Z_{0o} are obtained for each coupled section [1], [10]

$$Z_{0e} = Z_0 \frac{1 + k}{1 - k}, \quad Z_{0o} = Z_0 \frac{1 - k}{1 + k} \tag{8}$$

Where Z_0 is the system impedance (typically 50 Ω). These impedances are then converted to physical dimensions—namely the trace width W and spacing S between coupled lines—using standard coupled-line formulas or the conformal-mapping method outlined in [1]– [10]. The design is simulated on a Rogers substrate RO3006 ($\varepsilon_r = 6.5$, $h = 1.27$ mm, $\tan\delta = 0.002$), which allows for high impedance contrast and low insertion loss, enabling tight coupling in a compact layout. The gap-to-width ratio can be estimated by.

$$\frac{S}{w} = \frac{1}{\pi} \cosh^{-1}\left(\frac{Z_{0e} + Z_{0o}}{Z_{0e} - Z_{0o}}\right) \tag{9}$$

III. Simulation Results

Fig. 1 illustrates the proposed parallel-coupled microstrip bandpass filter designed to operate at 2.0 GHz for receiver (Rx) and 2.4 GHz for transmitter (Tx) applications. Each band features a 50 MHz bandwidth and exhibits a Chebyshev response with 0.1 dB passband ripple. The filter adopts a second-order topology, where the resonators are modeled as half-wavelength microstrip lines on a low-loss Rogers substrate. Each coupled section is precisely dimensioned to achieve the required even- and odd-mode impedances, with optimized width-to-height (W/h) and spacing-to-width (S/W) ratios derived from analytical models. Table I presents the final physical dimensions obtained after simulation-based optimization using AWR software.

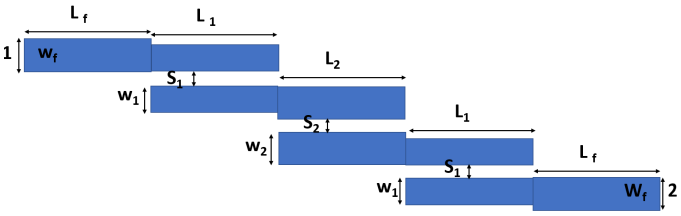

Fig. 1. Schematic of parallel-coupled microstrip BPF second order.

TABLE I
Physical Dimensions of Coupled Sections for Tx and Rx Filters.

Dimensions	BPF TX $f_0 = 2.4$GHz	BPF RX $f_0 = 2$ GHz
Length of feed (L_f)	7.64 mm	9.715 mm
Length of parallel coupling 1(L_1)	14.50 mm	17.68 mm
Length of parallel coupling 1(L_2)	14.49 mm	17.1 mm
Width of feed (W_f)	1.928 mm	1.89 mm
Width of parallel coupling 1 (W_1)	1.465 mm	1.63 mm
Width of parallel coupling 2 (W_2)	2.024 mm	2.152 mm
Spacing of parallel coupling 1(S_1)	0.897 mm	0.76 mm
Spacing of parallel coupling 2 (S_2)	2.93 mm	2.673 mm

Utilizing the dimensions presented in Table I within AWR, Fig. 2 illustrates the frequency response of the second-order bandpass filter in the RX band. The center frequency is 2 GHz, with a bandwidth of approximately 50 MHz at a return loss (S11) of 20 dB, as specified in the preceding section. The insertion loss measured 1 dB at the center frequency, with the initial spurious frequency occurring at 4 GHz. the selectivity is 0.075 and 0.15 dB/MHz on the upper side and lower sides, respectively

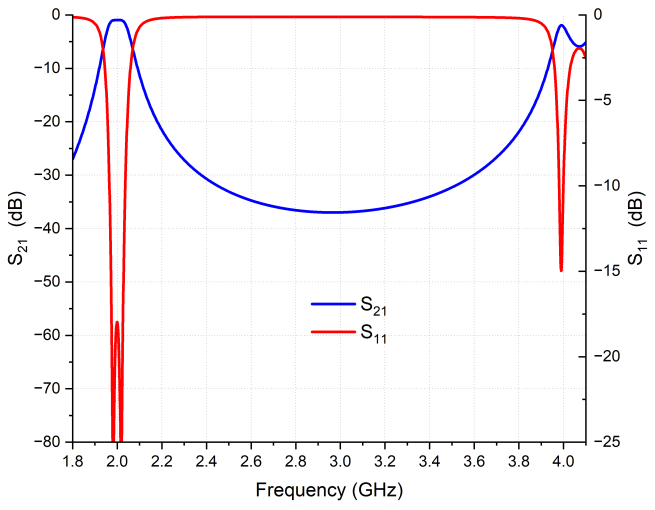

Fig. 2. Simulated response of second-order Chebyshev parallel-lined BPF at Rx band.

Fig.3 illustrates the frequency response within the Tx band. A perfect concordance between the analytical model and simulation in AWR is demonstrated, based on a resonant frequency of 2.4 GHz and a bandwidth of 50 MHz. The spurious window pertains to two. the TX band was 0.107 and 0.157 dB/MHz on the upper side and lower sides, respectively.

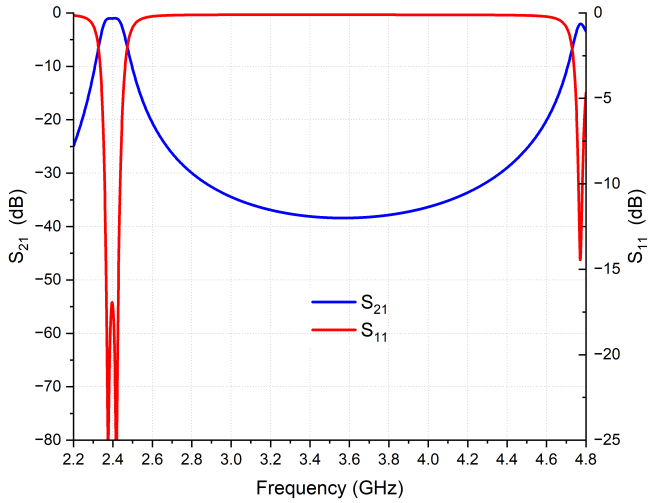

Fig. 3. Simulated response of second-order Chebyshev parallel-lined BPF at Tx band.

To determine the length of the 180° phase shift

$$\ell_{180^\circ} = \frac{\lambda_g}{2} \tag{10}$$

By connecting the two filters in a common port, a four-port diplexer configuration is obtained as shown in Fig. 4. The diplexer requires optimization when interconnecting the two filters due to the influence of the input impedance at the common port. Following the optimization of all diplexer parameters, table II presents the diplexer's dimensions.

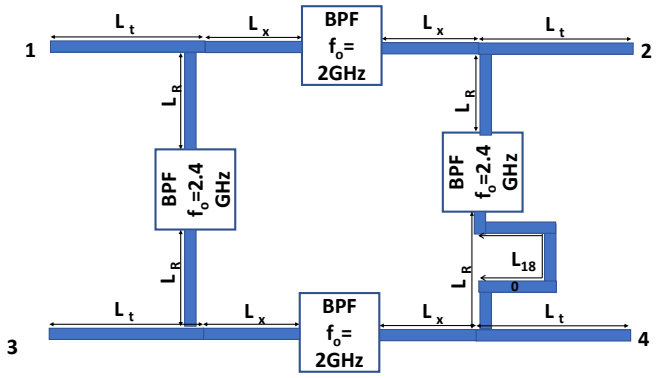

Fig. 4. The proposed Four port diplexer.

Fig.5 depicts the phase response of the two transmission paths, S_{13} and S_{24} , over the 2.30–2.50 GHz band with the target operation at 2.4 GHz. The key requirement for a 180° configuration coupling behavior is that the two corresponding outputs exhibit a 180° relative phase shift at the center frequency, which leads to response in Fig. 6.

TABLE II
PHYSICAL DIMENSIONS OF 4 PORT DIPLEXER.

Dimensions	BPF TX $f_0 = 2.4$GHz	BPF RX $f_0 = 2$ GHz
Length of feed (L_f)	7.699	9.545
Length of parallel coupling 1(L_1)	14.364	17.687
Length of parallel coupling 1(L_2)	14.985	17.1049
Width of feed (W_f)	1.928	1.8925
Width of parallel coupling 1 (W_1)	1.217	1.50
Width of parallel coupling 2 (W_2)	2.156	1.963
Spacing of parallel coupling 1(S_1)	0.7214	0.7461
Spacing of parallel coupling 2 (S_2)	2.8167	2.699
L_t	11.392	
L_x	7.357	
L_R	9.811	
L_{180}	29.5	

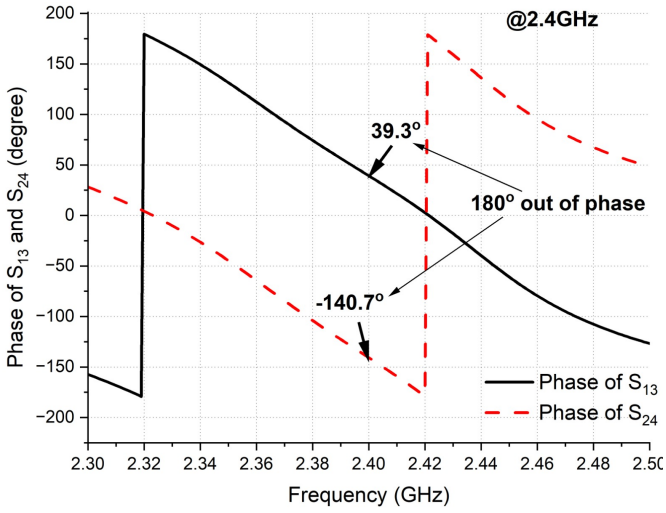

Fig. 5. Simulation results of phase S_{24} and S_{13} with a 180° phase difference at 2.4 GHz.

Fig. 6 illustrates the simulated response of a four-port diplexer. All bands are demonstrated to transmit at 2.4 GHz and receive at 2 GHz. The selectivity is elevated in the interval between the bands, with several transmission zeros present in each band to enhance isolation between them. The isolation measured 50 dB at 2 GHz and 78.5 dB at 2.4 GHz, as illustrated in Fig. 7. In comparison, the isolation was 30 dB when employing a single BPF. The variation in isolation between the bands is attributed to the design of phase 180 at the transmit (TX) band. Additionally, these values can be reversed by designing it at 2 GHz.

IV. EFFECTIVE MISMATCH ANTENNA IMPEDANCE

Due to multiple interacting factors—such as variations in antenna geometry, substrate properties, or loading conditions—the input impedance of the antenna can fluctuate, which in turn alters the impedance matching at the diplexer ports and degrades the isolation between its channels. From the Fig. 8, as the real part of the antenna impedance RA increases from about 40 Ω to 60 Ω, the isolation behavior of the diplexer changes noticeably. For the TX path, isolation rises steadily from 64 dB at 40 Ω to a peak of 85 dB near Ω , then drops back to about 69 dB at 60 Ω. In contrast,

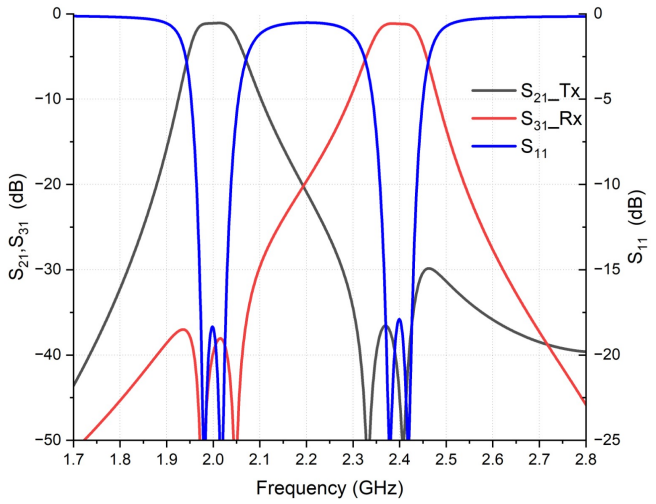

Fig. 6. The frequency response of 4port diplexer with 2nd order filters.

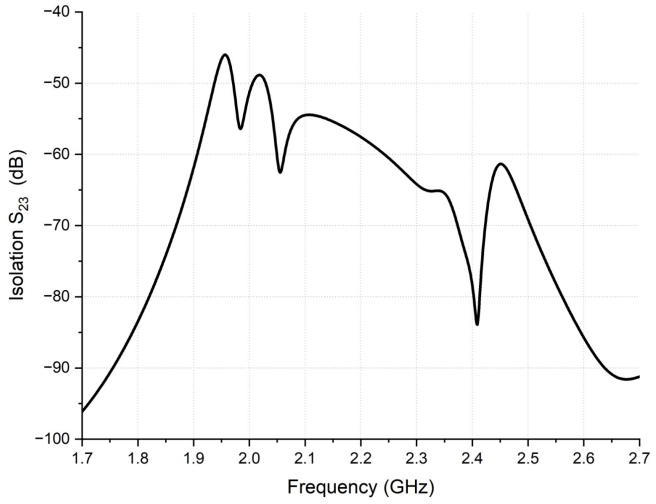

Fig. 7. The isolation of (S_{23}) 4port diplexer.

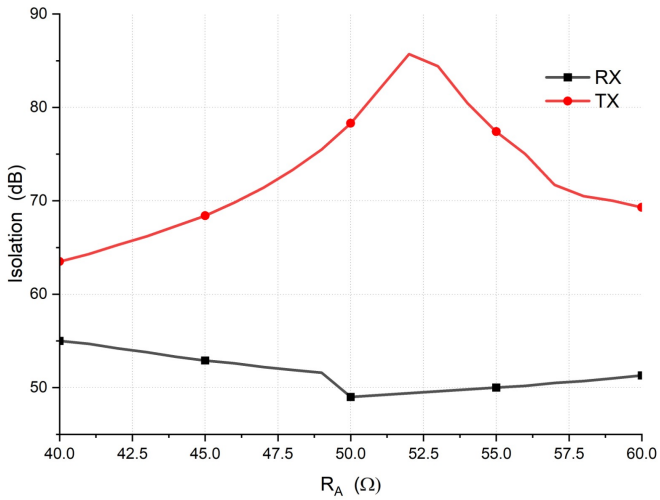

Fig. 8. The isolation of (S_{23}) 4port diplexer.

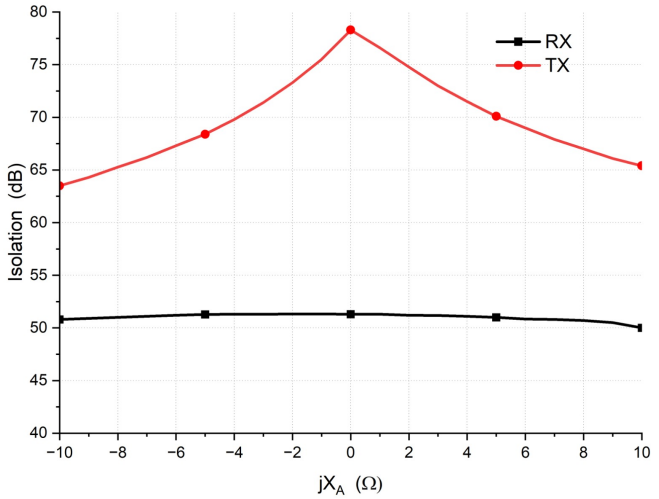

Fig. 9. The isolation of (S_{23}) 4port diplexer.

the RX path shows relatively minor variation, starting at 55 dB at 40 Ω, dipping to 49 dB around 50 Ω, and recovering slightly to 51 dB at 60 Ω. This indicates that changes in the real part of the antenna impedance can significantly affect diplexer isolation—especially for the TX channel—by altering the impedance matching and thus the port-to-port coupling characteristics.

From Fig. 9, as the imaginary part of the antenna impedance jX_A varies from -10 Ω to $+10$ Ω, the diplexer isolation also changes, but less dramatically than the real part. The TX path shows its highest isolation at zero reactance, peaking around 78 dB at $jX_A = 0$ Ω and gradually dropping toward 63–65 dB at the extreme reactances of ± 10 Ω. In contrast, the RX path remains nearly flat, with isolation fluctuating only slightly between about 50 dB and 51 dB across the entire reactance range. This behavior indicates that the diplexer is optimally matched for a near-zero reactive impedance; as the reactance becomes inductive or capacitive, the mismatch increases, reducing isolation—especially in the TX channel—while the RX channel remains comparatively insensitive.

The proposed architecture can exploit a variable impedance at Port 4 to fine-tune the isolation across the transmit and receive bands by compensating for either the real or the imaginary part of the antenna impedance. Simulation results indicate that when the load impedance Z_L at Port 4 is varied in the same manner as the antenna impedance, as shown in Fig. 10, the overall isolation characteristics remain essentially unchanged, demonstrating that the topology preserves high isolation even under coordinated impedance variations.

Figures 8–10 highlight a key novelty of this work: the proposed four-port diplexer is evaluated and co-designed at the antenna interface under realistic impedance variations, rather than only at the nominal 50 Ω condition. In Fig. 8, we map isolation versus the antenna resistance R_A (40–60 Ω) and show that the Tx isolation exhibits a clear optimum while the Rx isolation remains comparatively stable, revealing which path is most sensitive to resistive mismatch. In Fig. 9, we extend the robustness analysis to reactive mismatch and demonstrate

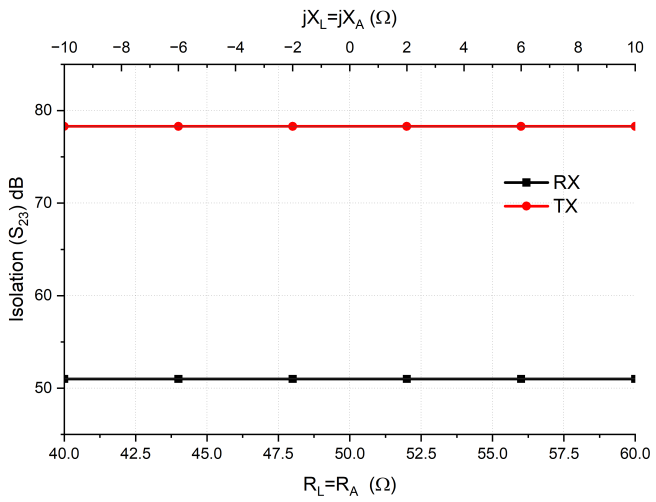

Fig. 10. The isolation of (S_{23}) 4port diplexer.

a broad maximum near $jX_A \approx 0$ with only modest Tx degradation toward $\pm 10\ \Omega$, confirming stable cancellation under capacitive/inductive loading. Finally, Fig. 10 demonstrates an impedance-control mechanism: when a controllable load Z_L at Port 4 is co-varied with the antenna impedance, the isolation remains essentially unchanged, indicating that the cancellation balance can be preserved under co-variate platform/user perturbations.

V. Discussion

The four-port diplexer–antenna architecture realizes isolation enhancement through amplitude–phase cancellation using a dedicated 180° inversion branch, while simultaneously constraining impedance sensitivity at the antenna interface. Simulation data indicate isolation plateaus of $\approx 50\,\text{dB}$ at 2.0 GHz (Rx) and 78.5 dB at 2.4 GHz (Tx) with second-order parallel-coupled bandpass filters on Rogers substrate RO3006 ($\varepsilon_r = 6.5$, $h = 1.27\,\text{mm}$, $\tan\delta = 0.002$) and $\approx 1\,\text{dB}$ in-band insertion loss; the first spurious response emerges near 4 GHz, and passband edge slopes are $\{0.075, 0.150\}$ dB/MHz (Rx, upper/lower) and $\{0.107, 0.157\}$ dB/MHz (Tx, upper/lower). Relative to a single-BPF baseline ($\sim 30\,\text{dB}$ isolation under match), the cancellation network yields multi-decade suppression without resorting to high-order filtering, corroborating that phase-balanced four-port topologies offer a favorable isolation–loss–footprint operating point. Load-sweep analyses clarify robustness mechanisms: variation of the antenna resistance R_A from $40\ \Omega \to 50\ \Omega \to 60\ \Omega$ drives Tx isolation ~ 64 dB $\to\sim 79$ dB $\to\sim 69$ dB, while Rx isolation drifts more mildly (~ 55 dB $\to\sim 49$ dB $\to\sim 51$ dB); reactance sweeps $jX_A \in [-10, +10]\ \Omega$ preserve a broad optimum at $jX_A \approx 0\ \Omega$ (Tx $\approx 78\,\text{dB}$) with only modest degradation toward the extremes (Tx $\approx$ 63–65 dB; Rx $\approx$ 50–51 dB). These trends imply that cancellation balance is primarily governed by real-part perturbations, and that the present interface co-design dampens reactance-induced imbalance. Geometry control of the inversion path (length $L_{180} \approx 29.5\,\text{mm}$) provides a practical tuning knob: assigning the phase-inversion branch to the alternate band flips which band attains the deeper isolation null, enabling application-specific prioritization of Tx or Rx protection. Coordinated variation of the port-4 load Z_L alongside the antenna impedance leaves isolation essentially invariant over the studied range, indicating that the topology's balance is preserved under co-variate platform perturbations. Overall, the evidence supports the use of four-port cancellation with impedance-aware interfacing as a compact route to stringent Tx/Rx coexistence, while highlighting a residual sensitivity to R_A that motivates closed-loop or adaptive balancing in environments with strong user or platform loading.

VI. Conclusion

A compact four-port diplexer–antenna front end with integrated impedance control has been demonstrated to deliver $\approx 50\,\text{dB}$ (2.0 GHz) and 78.5 dB (2.4 GHz) isolation using only second-order parallel-coupled BPFs and a 180° phase-inversion branch, with $\approx 1\,\text{dB}$ insertion loss and the first spurious near 4 GHz. Compared with a single-filter baseline ($\sim 30\,\text{dB}$ isolation), the co-designed cancellation network achieves substantial suppression without high-order selectivity or large footprint. Isolation remains high across realistic impedance sweeps, with dominant sensitivity to the antenna resistance and mild dependence on reactance; assigning the inversion path to either band allows designers to prioritize Tx or Rx protection. These results position four-port cancellation with impedance-aware interfacing as a practical building block for multi-band transceivers and MIMO platforms where stringent coexistence constraints apply.

References

[1] J. Konpang, M. Sandhu, N. Somjit, and I. C. Hunter, "Four-port diplexer for high tx/rx isolation for integrated transceivers," *IET Microwaves, Antennas & Propagation*, vol. 12, no. 6, pp. 1034–1040, May 2018.

[2] D. Zhang *et al.*, "A diplexer antenna with extremely high isolation for co-site applications," *AEU – International Journal of Electronics and Communications*, 2024, early access.

[3] M. A. Chaudhary, S. Roshani, and S. Shabani, "A miniaturized dual-band diplexer design with high port isolation for uhf/shf applications using a neural network model," *Micromachines*, vol. 14, no. 4, p. 849, 2023.

[4] S. Nandi and A. Mohan, "An siw cavity-backed self-diplexing antenna," *IEEE Antennas and Wireless Propagation Letters*, vol. 16, pp. 2708–2711, 2017.

[5] "Four-port dual-mode diplexer with high signal isolation," *Advances in Condensed Matter Physics*, 2020.

[6] N. Wattikornsirikul *et al.*, "Dual-mode diplexer with high isolation based on amplitude and phase cancellation technique," *Progress In Electromagnetics Research*, 2018.

[7] M. H. Almalki, A. Affandi, and A. Syed, "Design of dual-band, 4-ports mimo antenna-diplexer based on quarter-mode substrate integrated waveguide," *International Journal of Antennas and Propagation*, vol. 2022, no. 1, p. 4151038, 2022.

[8] R. Asaithambi *et al.*, "Self-diplexing siw rectangular cavity-backed antenna featuring high isolation," *Electronics*, 2025.

[9] P. PourMohammadi, H. Naseri, N. Melouki, F. Ahmed, T. A. Denidni, and G. A. E. Vandenbosch, "Highly-isolated compact self-diplexing antenna," *AEU – International Journal of Electronics and Communications*, p. 155025, 2024, article.

[10] S. W. O. Luhaib, N. Somjit, and I. C. Hunter, "Spurious stopband improvement of dual-mode dielectric resonator filters using t-shaped coupling probe," *IET Microwaves, Antennas & Propagation*, vol. 12, no. 15, pp. 2345–2349, Dec 2018.

[11] J. Tao *et al.*, "A phase canceling technique to improve saw duplexer isolation," *Applied Sciences*, 2023.

[12] "Four-port microstrip diplexer for rf interference rejection," Conf./Journal via ResearchGate, 2016–2018.
[13] S. W. O. Luhaib *et al.*, "Compact triple-mode microwave dielectric resonator filters," *International Journal of Electronics Letters*, vol. 8, no. 2, pp. 194–204, Apr 2020.
[14] F. E. Mahmood, H. M. AlSabbagh, and R. Edwards, "Cpw-fed uwb antenna with band-notch by hexagonal shape slot," in *2012 International Conference on Future Communication Networks*. IEEE, 2012, pp. 69–71.
[15] A. T. Hussein and S. Luhaib, "Designing e-shape microstrip patch antenna in multilayer structures for wifi 5 ghz network," in *Proc. 20th Telecommunications Forum (TELFOR)*, Belgrade, Serbia, Nov 2012.
[16] H. M. AlSabbagh and et.al, "A uwb fractal antenna for body area network applications," in *2012 Loughborough Antennas & Propagation Conference (LAPC)*. IEEE, 2012, pp. 1–4.
[17] F. E. Mahmood and S. W. O. Luhaib, "Semi-circular compact cpw-fed antenna for ultra-wideband applications," *TELKOMNIKA (Telecommunication Computing Electronics and Control)*, vol. 20, no. 6, pp. 1200–1205, 2022.

Saad Wasmi Osman Luhaib received the B.Sc. and M.Sc. degrees in Electronic and Communication Engineering from the University of Mosul, Iraq, in 2004 and 2007, respectively, and the Ph.D. degree in Communication Engineering from the University of Leeds, U.K., in 2018. He is currently an Assistant Professor with the Department of Electrical Engineering, University of Mosul. His research interests include microwave engineering, antennas, filters, multimode resonators, and communication systems.
email:saadw1981@gmail.com

Farhad E. Mahmood received the B.S. and M.S. degrees from the University of Mosul, in 2005, and 2008, respectively, and received the Ph.D. degree from The University of Kansas, the USA in 2019, all in electrical engineering University of Mosul. Dr. Mahmood is with the department of Communications and Intelligent Digital Systems Engineering. His research interests include wireless communications, energy efficiency, Machine learning, and signal processing. Dr. Mahmood is a reviewer in several IEEE transaction journals. He can be contacted at email: farhad.m@uomosul.edu.iq

Shamil H. Hussein is an Assistant Professor in the Department of Electrical Engineering at the University of Mosul, specializing in RF circuit design and energy harvesting. He holds a Ph.D., M.Sc., and B.Sc. in Electrical Engineering from the University of Mosul. Alnajjar has extensive teaching and research experience and has published numerous papers on neural networks, power amplifiers, and energy harvesting systems. He is proficient in MATLAB, ADS, CST, and SILVACO ATLAS.